Charge Recombination Kinetics and Protein Dynamics in Wild Type and Carotenoid-less Bacterial Reaction Centers: Studies in Trehalose Glasses

ARTICLE *in* THE JOURNAL OF PHYSICAL CHEMISTRY B · AUGUST 2009

Impact Factor: 3.3 · DOI: 10.1021/jp902287y · Source: PubMed

4 AUTHORS, INCLUDING:

Marco Malferrari
University of Bologna
19 PUBLICATIONS **60** CITATIONS
SEE PROFILE

Giovanni Venturoli
University of Bologna
110 PUBLICATIONS **1,941** CITATIONS
SEE PROFILE

Charge Recombination Kinetics and Protein Dynamics in Wild Type and Carotenoid-less Bacterial Reaction Centers: Studies in Trehalose Glasses

Francesco Francia,[†] Marco Malferrari,[†] Sophie Sacquin-Mora,[‡] and Giovanni Venturoli*[,†,§]

Laboratorio di Biochimica e Biofisica, Dipartimento di Biologia, Università di Bologna, 40126 Bologna, Italy, Laboratoire de Biochimie Théorique, CNRS UPR 9080, Institut de Biologie Physico-Chimique, 75005 Paris, France, and Consorzio Nazionale Interuniversitario per le Scienze Fisiche della Materia (CNISM), Bologna, Italy

Received: March 14, 2009; Revised Manuscript Received: June 11, 2009

The coupling between electron transfer and protein dynamics has been investigated in reaction centers (RCs) from the wild type (wt) and the carotenoid-less strain R26 of the photosynthetic bacterium *Rhodobacter sphaeroides*. Recombination kinetics between the primary photoreduced quinone acceptor (Q_A^-) and photoxidized donor (P^+) have been analyzed at room temperature in RCs incorporated into glassy trehalose matrices of different water/sugar ratios. As previously found in R26 RCs, also in the wt RC, upon matrix dehydration, $P^+Q_A^-$ recombination accelerates and becomes broadly distributed, reflecting the inhibition of protein relaxation from the *dark-adapted* to the *light-adapted* conformation and the hindrance of interconversion between conformational substates. While in wet trehalose matrices (down to ∼one water per trehalose molecule) $P^+Q_A^-$ recombination kinetics are essentially coincident in wt and R26 RCs, more extensive dehydration leads to two-times faster and more distributed kinetics in the carotenoid-containing RC, indicating a stronger inhibition of the internal protein dynamics in the wt RC. Coarse-grained Brownian dynamics simulations performed on the two RC structures reveal a markedly larger flexibility of the R26 RC, showing that a rigid core of residues, close to the quinone acceptors, is specifically softened in the absence of the carotenoid. These experimental and computational results concur to indicate that removal of the carotenoid molecule has long-range effects on protein dynamics and that the structural/dynamical coupling between the protein and the glassy matrix depends strongly upon the local mechanical properties of the protein interior. The data also suggest that the conformational change stabilizing $P^+Q_A^-$ is localized around the Q_A binding pocket.

Introduction

The photosynthetic reaction center (RC) of the purple bacterium *Rhodobacter* (*Rb.*) *sphaeroides* is considered to be an excellent model system for investigating the relationship between protein internal motions and long-range electron transfer. Following photoactivation, this integral pigment−protein complex catalyzes a sequence of electron transfer reactions leading to charge separation across the dielectric of the intracytoplasmic membrane.[1−3] Within the RC, photon energy is absorbed by a bacteriochlorophyll dimer, P, situated near the periplasmic side of the protein. P is promoted to the first excited singlet state and acts as the primary electron donor, transferring an electron, via an interposed bacteriopheophytin molecule, to the primary quinone acceptor, Q_A, located 25 Å away from P and closer to the cytoplasmic side of the RC. This photoactivated electron transfer process generates in about 200 ps the primary charge separated state $P^+Q_A^-$ of the RC. In the absence of the secondary quinone acceptor molecule, Q_B (or in the presence of inhibitors which block electron transfer from Q_A^- to Q_B), the RC returns to its ground state by direct electron tunneling from Q_A^- to P^+.[4]

A number of investigations, exploiting independent spectroscopic, electrometric, and biochemical approaches,[5−13] indicate coherently that, following the light-induced primary charge separation, the RC protein−solvent system responds to the generated electric field by relaxing from a *dark-adapted* to a *light-adapted* conformation which stabilizes the charge separated $P^+Q_A^-$ state relative to the PQ_A ground state. Fundamental information on the interplay between this RC conformational dynamics and electron transfer has been provided by low temperature studies of $P^+Q_A^-$ recombination kinetics.[5,9,10,13] In a pioneering study, Kleinfeld and co-workers[5] showed that the recombination kinetics is accelerated by a factor of 5, with respect to room temperature, when RCs are frozen to 77 K *in the dark*; at variance, the above process is sizably slowed down when cooling takes place *in the light*. This behavior was interpreted as reflecting the trapping at low temperature of the *dark-adapted* or the *light-adapted* conformation. Both conformations consist of a large ensemble of substates, as inferred by the strongly distributed kinetics of charge recombination at cryogenic temperatures.[5,10] More recently, the kinetics of $P^+Q_A^-$ recombination have been systematically examined as a function of temperature (5−300 K), illumination protocol, and warming rate.[10] In this study a quantitative analysis of the coupling between electron transfer and protein motions was developed, based on a quantum-mechanical electron transfer model (Fermi's golden rule and the spin-boson model). The static heterogeneity of the protein ensemble, conformational relaxations, and fluctuations between conformational substates were all cast onto a single parameter, the energy gap between the charge separated ($P^+Q_A^-$) and the neutral (PQ_A) states, which was mapped on a single conformational coordinate along which the RC protein

* To whom correspondence should be addressed. E-mail: giovanni.venturoli@unibo.it. Phone: +39-051-2091288. Fax: +39-051-242576.

[†] Università di Bologna.

[‡] Institut de Biologie Physico-Chimique.

[§] Consorzio Nazionale Interuniversitario per le Scienze Fisiche della Materia (CNISM).

10.1021/jp902287y CCC: $40.75
Published on Web 07/08/2009

performs slow, diffusive motions.[10] The model accounts quantitatively for the behavior observed over the whole accessible temperature range in native[10] and generically modified RCs,[13] in a water-glycerol solvent, and in RCs trapped in a sol−gel matrix.[14] According to this dynamic model,[10] at physiological temperatures, the RC protein, following light-induced transition to the $P^+Q_A^-$ state, relaxes rapidly from the *dark-adapted* to the *light-adapted* conformation, solvating the altered charge distribution. This relaxation is associated with a decrease in the energy gap between $P^+Q_A^-$ and the PQ_A ground state, which is reflected in a decrease of the electron transfer rate, i.e. in the stabilization of the charged separated state. At room temperatures, moreover, the RC protein rapidly samples the conformational substate ensemble, so that averaging of the corresponding rate distribution occurs over the time scale of charge recombination. This gives rise to an almost exponential kinetics of $P^+Q_A^-$ recombination (lifetime, $\tau \approx 10^{-1}$ s). At variance, freezing RCs in the dark at temperatures between 250 and 150 K hampers progressively the relaxation from the *dark-adapted* to the stabilized, *light-adapted* conformation, as well as the interconversion between conformational substates: this hindrance of the conformational dynamics results in a progressive increase of the average rate constant for $P^+Q_A^-$ recombination and in a progressively broader distribution of rate constants.[10] In summary, it appears that the recombination kinetics of the primary charge separated state is a sensitive probe of the associated internal RC dynamics.

In previous work we have shown that these dynamics of the RC can be modulated *at room temperature* by incorporating the RC into dehydrated amorphous trehalose matrices.[15] We have found, in fact, that in RCs purified from *Rb. sphaeroides* R26, embedded into trehalose glassy matrices, the kinetics of $P^+Q_A^-$ recombination abruptly accelerates and becomes broadly distributed when the content of residual water of the matrix is reduced below a threshold value. This behavior has been taken to indicate that, due to the strong structural/dynamical coupling between the RC protein and the solid trehalose glass, the thermal fluctuations between conformational substates and the relaxation to the *light-adapted* state are strongly hindered even at room temperature over the time-scale of charge recombination. In accordance with the dynamic model described above,[10] the drastic inhibition of the RC dynamics results in a strongly accelerated and distributed kinetics of $P^+Q_A^-$ recombination, which mimics *at room temperature* the one observed at cryogenic temperatures. This interpretation has been confirmed by successive studies, which showed that also the electron transfer from Q_A^- to Q_B is strongly affected by incorporation of the RC into trehalose glassy matrices. Upon dehydration of the matrices, this conformationally gated electron transfer[16] is arrested in a progressively increasing fraction of the reaction center population, and complete inhibition is attained in relatively wet glasses.[17] The dynamical origin of the effects observed on electron transfer is further corroborated by the finding that continuous preillumination (lasting from 10^{-3} to 10 s) of the RCs embedded into trehalose glasses causes a partial and progressive reversion of the effects observed on both $P^+Q_A^-$ recombination[18] and Q_A^- to Q_B electron transfer,[17] indicating that under these conditions the RC is gaining a limited conformational freedom. Notably the structural integrity and the photochemical activity of the RCs embedded in dried trehalose matrices are preserved at room temperature for long periods,[19] showing that incorporation into trehalose glassy matrices also inhibits large-scale dynamics, preventing the RC from exploring non-native conformations along the route to denaturation.

The observations summarized above are fully consistent with a large body of results obtained in soluble proteins and aimed at characterizing the dynamics of trehalose−water−protein systems, also in relation to the known peculiar efficacy of trehalose in the preservation of biostructures.[20] Both molecular dynamics simulations[21] and spectroscopic studies (time-resolved optical spectroscopy, FTIR spectroscopy, neutron scattering, Mössbauer, X-ray absorption spectroscopy) performed on myoglobin[22−26] and cytochrome *c*[27] containing trehalose matrices have shown that the residual water content strongly modulates the protein motional freedom. To explain the peculiar bioprotective effect of trehalose and the molecular mechanism by which the trehalose−water matrix inhibits protein dynamics, several factors have been considered as determinants: (i) stabilization via hydrogen bond formation between the sugar and the biostructure (*water-replacement hypothesis*);[28,29] (ii) trapping of residual water molecules at the biomolecule−sugar interface by glass formation (*water-entrapment hypothesis*);[30] and (iii) the dramatic increase in viscosity upon glass formation (*high-viscosity hypothesis*).[31] Although the mechanisms mentioned above are not necessarily mutually exclusive, they postulate that different protein−matrix interactions are predominantly responsible for bioprotection. According to the *water-replacement hypothesis*, replacement of the lost hydration layer by direct sugar−protein hydrogen bonding prevents dehydration-induced protein inactivation. At variance, the *water-entrapment hypothesis* proposes that the residual water molecules concentrated close to the biostructure preserve to a large extent its solvation and therefore native properties. Finally, the *high-viscosity hypothesis* suggests that the vitrifying sugars protect biostructures through the formation of extremely viscous glasses, thereby reducing the internal protein dynamics tied to the fluctuations in the bulk solvent.

Molecular dynamics simulations of myoglobin−water−trehalose systems indicate that in trehalose−water matrices the protein is constrained within a network of hydrogen bonds in which water molecules at the protein−matrix interface are simultaneously connected with protein surface residues and with matrix trehalose molecules.[32] Simulations have shown that the fraction of water molecules involved in such hydrogen bond networks increases upon decreasing the content of residual water. Accordingly, it has been proposed (*anchorage hypothesis*) that this hydrogen bond network, which locks the protein surface, is mainly responsible for coupling the internal dynamics of the protein to that of the glassy matrix.[19,20,33] The inhibition of internal protein dynamics, caused by extensive dehydration of the system, would reflect a tighter anchorage of the protein surface to an increasingly stiffer matrix. The *anchorage hypothesis* is in line with the *water-entrapment hypothesis*, since both models imply that the residual water molecules concentrate upon drying at the protein−matrix interface. In the *anchorage hypothesis*, however, the bioprotective effect of the entrapped water is not simply related to the preservation of the native solvation. According to the *anchorage hypothesis*, the water molecules confined at the protein surface are involved in multiple hydrogen bonding, which connects surface protein residues with sugar molecules, forming a mechanical network whose rigidity increases upon decreasing the water content of the system. Therefore, according to the *anchorage hypothesis*, the bioprotective effect arises primarily from the inhibition of the internal protein motions due to the mechanical constraints introduced at the surface of the biomolecule.

The *anchorage* model accounts for a number of observations both in myoglobin−water−sugar and in RC−water−sugar

matrices.[19,20,33] In the RC system, it has been recently observed that, at variance with trehalose, sucrose matrices are ineffective in blocking the RC dynamics coupled to charge recombination and in protecting the RC against thermal inactivation.[19] This remarkable finding can be rationalized in the context of the *anchorage hypothesis* when considering that sucrose, as compared to trehalose, has fewer sites available to form intermolecular hydrogen bonds with its surroundings.[34,35] As a consequence, in the sucrose matrices, the RC conformational dynamics is essentially uncoupled from that of the embedding sugar glass, in spite of the extreme viscosity and hardness of the dehydrated matrix. This observation argues strongly against the *high-viscosity* hypothesis. The idea that the bioprotection offered by trehalose is due to its ability to immobilize the protein surface through a thin, constrained layer of water has been recently supported by vibrational echo experiments and molecular dynamics simulations performed on different heme proteins.[36]

An implication of the *anchorage* model is that, for a given structural/dynamical coupling between the protein surface and the sugar matrix, the extent of inhibition of the *internal* protein dynamics is expected to depend on the *internal* protein rigidity. The local mechanical properties of the protein, in fact, will determine the structural/dynamical coupling between the matrix-locked surface and internal regions or sites of the protein. This consideration led us to compare the kinetics of $P^+Q_A^-$ recombination in dehydrated trehalose matrices embedding reaction centers purified from the carotenoid-containing wt strain 2.4.1 or from the carotenoid-less strain R26. High-resolution crystallographic structures are available for both the spheroidene containing 2.4.1[37] and the carotenoid-less RC.[38] They indicate that in the absence of the carotenoid, which is noncovalently bound at the M subunit, on the donor side of the RC, a detergent molecule is sitting in the middle of the carotenoid binding site. Comparative, high-pressure studies of the two RCs have shown that the carotenoid-containing structure is more compact than that of the R26 strain, suggesting in the latter a locally larger compressibility.[39,40] These two structures seem therefore to provide a suitable tool to examine the effects of an internal void in the protein structure on protein flexibility and on the matrix−protein dynamical coupling, as probed by the kinetics of $P^+Q_A^-$ recombination.

In this work we show that incorporation into extensively dehydrated trehalose matrices leads to a significantly faster and more distributed kinetics of charge recombination in the carotenoid-containing reaction center. This observation is consistent with the results of coarse-grained Brownian dynamics simulations performed on the two RC protein structures, which reveal a considerably higher rigidity of the carotenoid-containing RC.

Materials and Methods

RC Purification, Sample Preparation and Evaluation of the Water Content of Matrices. The carotenoid-containing RC was purified from *Rb. sphaeroides* strain 2.4.1 membranes following essentially the procedure described in ref 41. The RC from the R26 mutant was purified as described in ref 42.

α,α-Trehalose dihydrate (>99% purity) from Sigma-Aldrich (St. Louis, MO) was used without any additional purification. RC-trehalose glasses, in a fixed (sugar/RC protein) molar ratio equal to 10^4, were prepared according to the following procedure. RCs were suspended at 40 μM concentration in 10 mM Tris buffer, pH 8.0, 0.4 M trehalose, 0.025% LDAO, 10 mM *o*-phenanthroline. This inhibitor blocks Q_A^- to Q_B electron transfer,[43] thus allowing the recombination kinetics of the flash-induced $P^+Q_A^-$ state to be monitored. A thin layer (0.24 mL) of the trehalose-RC solution was deposited on a 50 mm diameter optical glass window and dried in a desiccator under N_2 flow at room temperature. In about 4 h, a glassy sample was obtained, which still contained a significant amount of residual water ($\approx 1.2 \times 10^4$ H_2O molecules per RC). Further dehydration of the trehalose sample was achieved by alternating incubation under an N_2 atmosphere at 30 °C for about 12 h and under vacuum for approximately the same time. The maximum dehydration was attained after several days of incubation. During spectroscopic measurements, to avoid water exchange between the sample and the environment, the optical window on which the RC−trehalose glassy matrix was formed was inserted into a specifically designed gastight sample holder, filled with dry N_2. Dried RC films were prepared using a similar procedure, except that trehalose was not added to the RC detergent suspension. In the absence of the sugar, extensive dehydration was obtained already after the initial desiccation under N_2 flow for about 4 h. Following this treatment, residual water was reduced to levels undetectable by near infrared (NIR) spectroscopy (see below). Before measuring $P^+Q_A^-$ recombination, RC films were further incubated under N_2 atmosphere for 2 days at room temperature.

The water content of RC−trehalose matrices was evaluated by NIR spectroscopy from the area of the combination band of water centered at ∼1940 nm. The RC absorption band at 802 nm was used as an internal standard to determine the molar H_2O/RC ratio, as described in detail in ref 15.

Measurements in solution were performed at a RC concentration ranging between 1 and 2 μM in 10 mM Tris, pH 8.0, 0.025% LDAO, and 10 mM *o*-phenanthroline.

Flash Absorption Spectroscopy and Kinetic Analysis of $P^+Q_A^-$ Recombination. The kinetics of recombination of the flash-generated $P^+Q_A^-$ state was recorded at 422 nm[44] using an apparatus for time-resolved absorption spectroscopy of local design.[19] Pulsed excitation was provided by a frequency doubled Nd:YAG laser (Handy 710, Quanta System, Milano, Italy) which delivers 200 mJ pulses of 7 ns width. From two to eight kinetic recordings were averaged depending on the signal-to-noise ratio in the sample. During averaging, the sample was allowed to dark adapt for at least 1 min between successive single photoexcitations.

The kinetics of $P^+Q_A^-$ recombination in RC embedded into trehalose matrices exhibit a clear nonexponential character, which becomes progressively more pronounced upon dehydration of the sample. As previously reported,[15,18,19] description of the survival probability $N(t)$ of the $P^+Q_A^-$ state after the photoexcitation pulse requires a continuous distribution $p(k)$ of rate constant k, i.e.:

$$N(t) = \frac{P^+Q_A^-(t)}{P^+Q_A^-(0)} = \frac{\Delta A_{422}(t)}{\Delta A_{422}(0)} = \int_0^\infty p(k)\ e^{-kt}\, dk \tag{1}$$

where $\Delta A_{422}(t)$ is the absorbance change recorded at 422 nm at time t, and $t = 0$ is the time at which the laser pulse is fired. Following the approach outlined in ref 45, first adopted by Feher and co-workers[5] to analyze $P^+Q_A^-$ recombination kinetics in RCs frozen at cryogenic temperature, we fitted the decay of the $P^+Q_A^-$ state to a power law of the form:

$$N(t) = (1 + k_0 t)^{-n} \tag{2}$$

with k_0 and n as free parameters. This parametrization in the time domain has the advantage that the corresponding distribution function $p(k)$, i.e. the inverse Laplace transform of $N(t)$ (see eq 1), can be obtained analytically,[46] that is

$$p(k) = \frac{k^{n-1}}{k_0^n}\frac{\exp(-k/k_0)}{\Gamma(n)} \quad (3)$$

where $\Gamma(n)$ is the gamma function and k_0 and n are related to the average rate constant, $\langle k\rangle$, and to the variance, σ,[2] of the distribution by

$$\langle k\rangle = nk_0 \qquad \sigma^2 = nk_0^2 \quad (4)$$

We have found that, under all the conditions considered (solutions, RC-film, RC-trehalose glassy matrices), the approach described above gave an adequate description of $P^+Q_A^-$ recombination kinetics.

Fitting of recombination kinetics to eq 2 was performed by least-squares minimization routines, based on a modified Marquardt algorithm.[47] Confidence intervals of the fitting parameters (average rate constant, $\langle k\rangle$, and width, σ, of the distribution function) were evaluated numerically through an exhaustive search method.[48,49] A series of nonlinear χ^2 minimizations was performed by varying stepwise the value of each ith fitting parameter, allowing the remaining fitting parameters to adjust. The obtained minimized χ^2 values were plotted versus the value of the ith parameter, obtaining an error graph for each ith fitting parameter. The confidence interval was calculated by using an F-statistic to evaluate the probability of a given fractional increase in χ^2 according to

$$\chi^2/\chi^2_{\min} = 1 + [m/(n-m)]F(m, n-m, 1-p) \quad (5)$$

where m is the number of parameters, n is the number of data points, and F is the upper $(1-p)$ quantile for Fisher's F distribution with m and $(m-n)$ degrees of freedom. Confidence intervals within two standard deviations ($p = 0.95$) are given (see the legends of Figures 1 and 2).

In order to test the reliability of extracting the $\langle k\rangle$ and σ values of the rate distribution function by the approach described above, we have additionally and independently characterized $p(k)$ using the method of cumulants, already introduced by us in the analysis of $P^+Q_A^-$ recombination kinetics.[15] In practice, the normalized experimental kinetics, $N(t)$, have been fitted to the third order cumulant expansion

$$N(t) = \exp(-<k>t + \mu_2 t^2/2! - \mu_3 t^3/3!) \quad (6)$$

where $\mu_2 \equiv \sigma^2$ is the variance and the third moment μ_3 provides a measure of the skewness or asymmetry of the monomodal rate distribution. The inclusion of higher order moments into eq 6 did not improve significantly the quality of the fit. The cumulant analysis and the power law approaches provided consistent $\langle k\rangle$ and σ values (see Results).

Redox Titrations of the P^+/P Couple in RC Detergent Suspensions. The P^+/P redox midpoint potentials of RCs purified from the 2.4.1 and R26 strains were determined by chemical oxidation−reduction titrations, essentially as described in ref 50. At a given ambient redox potential (E_h), the degree of reduction of the primary electron donor was measured by monitoring spectrophotometrically the maximal extent of P photoxidation induced in the RC suspension by a train of six flashes fired 100 ms apart. The extent of P photoxidation was measured from the absorbance change induced at 542 nm (ΔA_{542}). Excitation was provided by a xenon flash lamp (3.25 J discharge energy, 4 μs pulse duration at half-maximal intensity) screened by a Kodak Wratten 88A filter. E_h was measured with a platinum electrode and a calomel reference electrode, calibrated using equimolar ferri/ferrocyanide mixtures.[51] The potential was adjusted by the addition of small volumes of concentrated potassium ferricyanide or Na ascorbate solutions. Titrations were performed at RC concentrations ranging between 0.5 and 2.0 μM in 20 mM Tris, pH 8.0, 60 mM KCl, in the absence and in the presence of the redox mediators 2,3,5,6-tetramethyl-*p*-phenylene diamine (DAD) and *p*-benzoquinone (pBQ) at 20 μM concentrations. To compare with previously published results,[52] titrations of the wt RCs were also performed in the presence of 0.1% Triton X-100 and 1 mM EDTA. Equilibration between the redox center P and the platinum electrode was assessed by verifying reversibility during an oxidative and a successive reductive titration.

The midpoint potential (E_m) was obtained by fitting the titrations to the one electron Nernst equation:

$$\Delta A_{542}(E_h) = \Delta A_{542}^{\max}/\left\{1 + \exp\left[\frac{F(E_h - E_m)}{RT}\right]\right\} \quad (7)$$

where E_h is the ambient redox potential relative to the hydrogen electrode, R and F are the gas and Faraday constants, respectively, and T is the absolute temperature. The free parameters were the midpoint potential, E_m and $\Delta A_{542}^{\max}$, defined as the expected absorbance change induced by the train of flashes in a fully reduced sample.

Brownian Dynamics Simulations. To compare the flexibility of the 2.4.1 RC and of the R26 mutant, Brownian dynamics simulations have been carried out essentially as described in ref 53. The simulations adopted a coarse-grained protein model,[54,55] in which each amino acid is represented by one pseudoatom located at the Cα position, and small side chains (with the exception of Gly) have a second pseudoatom at the geometric center of the heavy atoms of the side chain, while larger side chains (Arg, Gln, Glu, His, Lys, Met, Trp, Tyr) have a pseudoatom at the center of the Cβ−Cγ bond and a third pseudoatom at the geometrical center of the heavy atoms of the side chain atoms beyond Cγ. Interactions between the pseudoatoms are treated according to the standard elastic network model;[56] that is, all pseudoatoms lying closer than 9 Å are joined with quadratic springs having the same force constant of 0.6 kcal mol^{-1} Å^{-2}. Springs are assumed to be relaxed in the reference conformation of the protein, derived from the crystallographic data. Brownian dynamics simulations use an implicit solvent description via the diffusion and random displacement terms in the equation of motion.[57] Other details of the simulation procedure are given in ref 55.

From the positional fluctuations resulting from Brownian dynamics simulations, carried out for 50,000 steps at a temperature of 300 K, effective force constants for displacing each particle i are calculated as

$$k_i = \frac{3k_BT}{\langle (d_i - \langle d_i\rangle)^2\rangle} \quad (8)$$

where brackets ⟨⟩ indicate an average taken over the whole simulation, k_B is the Boltzmann constant, and d_i is the average distance of particle i from the other particles j in the protein, excluding the pseudoatoms, which belong to the same residue m to which particle i belongs. Also, the distances between the Cα pseudoatom of residue m and the Cα pseudoatoms of the adjacent residues $m + 1$ and $m - 1$ are not included in the average. The force constant associated with each residue m is taken to be the average of the force constants calculated according to eq 8 for each of the pseudoatoms i forming this residue. Within this framework, the mechanical properties of the protein are described at the residue level by its "rigidity profile", i.e. by the ordered sequence of the force constants calculated for each residue.

Results

Kinetics of $P^+Q_A^-$ Recombination in RC−Trehalose Glasses and Dried RC Films. We have compared the room temperature kinetics of $P^+Q_A^-$ recombination after a laser pulse in RCs purified from the carotenoid-containing wt strain and from the carotenoid-less mutant R26 under different environmental conditions, which are known to affect markedly the RC dynamics coupled to the reaction.[15,18,19] Figure 1 shows the kinetics recorded in solution, in a RC film extensively dehydrated (panel A), and in a RC−trehalose glassy matrix characterized by an extremely low content of residual water (panel B). As previously observed in R26 reaction centers, under all the conditions tested, kinetics are accurately described by a power law (eq 2). Accordingly, the kinetic process can be fully characterized by a gamma distribution of rate constants (eq 3), as described in detail in the Materials and Methods section.

In solution, the kinetics recorded in the wt and in the R26 RCs essentially coincide, marginally deviating from an exponential decay, as is shown by the narrow rate distributions (Figure 1C). The values obtained for the average rate constant, $\langle k \rangle$, and for the rate distribution width, σ, are close to 11 s^{-1} and 2 s^{-1}, respectively, for both strains, in agreement with previous data obtained in the R26 mutant.[15,18,19] When the RC suspensions are extensively dehydrated, obtaining RC films, the recombination kinetics accelerate in both wt and R26 RCs

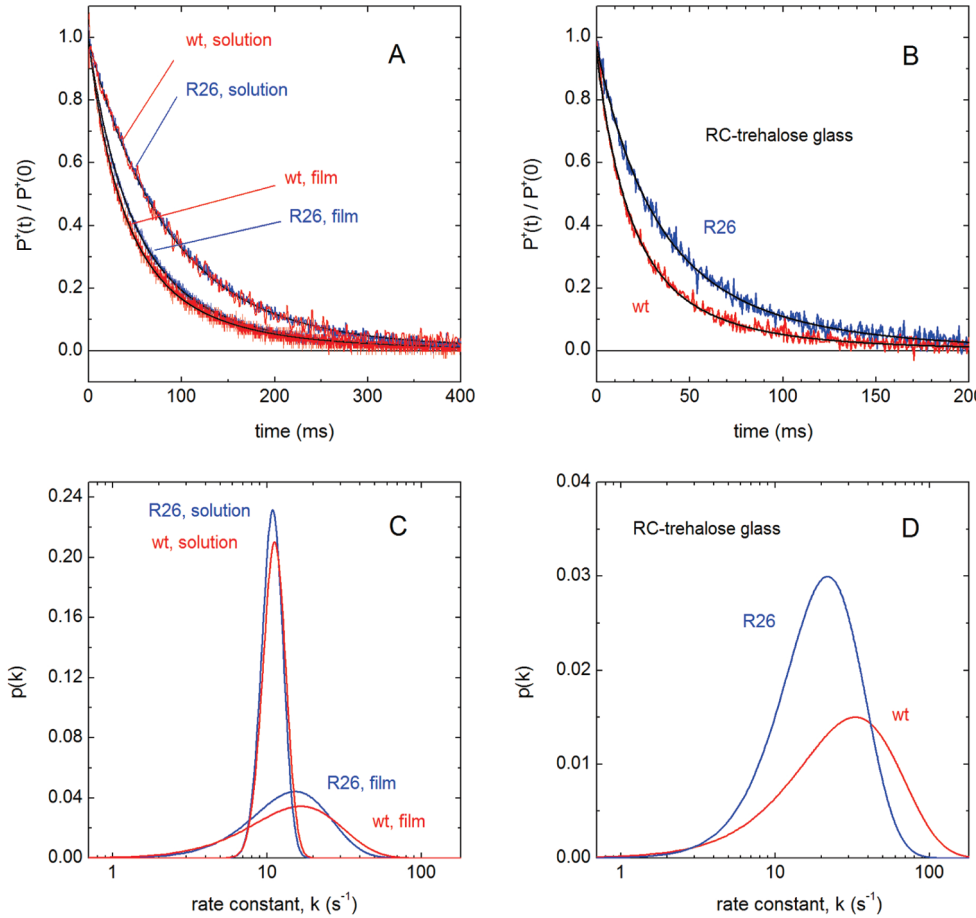

Figure 1. Kinetic analysis of $P^+Q_A^-$ recombination following flash excitation of RC purified from the wt 2.4.1 and the R26 mutant of *Rhodobacter sphaeroides* measured under different environmental conditions. The decays of the absorbance change induced at 422 nm by a laser pulse have been measured at $T = 21$ °C in detergent RC solution (panel A), in dehydrated RC films (panel A), and in extensively dried trehalose-RC glassy matrices (panel B). Note the different scales in panels A, C and B, D. Traces recorded in the wt and in the R26 RC are shown in red and blue, respectively. Kinetics have been normalized to the maximal change immediately after photoexcitation ($t = 0$). Best fits to eq 2 are shown as black continuous lines. The corresponding rate distributions (see eq 3) are shown in the lower panels (C and D). The values obtained for the average rate constant $\langle k \rangle$ and the distribution width σ (see eq 4) are reported in the following, with the extremes of the calculated confidence intervals within two standard deviations indicated in brackets. Panel A: wt, solution $\langle k \rangle = 11.5$ (11.3, 11.8) s^{-1}, $\sigma = 1.9$ (0.0, 3.4) s^{-1}; R26, solution $\langle k \rangle = 11.1$ (11.0, 11.3) s^{-1}, $\sigma = 1.1$ (0.0, 1.9) s^{-1}; wt, film $\langle k \rangle = 24.0$ (23.9, 24.6) s^{-1}, $\sigma = 13.4$ (11.3, 16.3) s^{-1}; R26, film $\langle k \rangle = 20.3$ (20.2, 20.5) s^{-1}, $\sigma = 10.2$ (10.0, 10.3) s^{-1}. Panel B: wt RC−trehalose glass $\langle k \rangle = 52.3$ (47.4, 57.6) s^{-1}, $\sigma = 32.0$ (26.2, 37.4) s^{-1}; R26 RC−trehalose glass $\langle k \rangle = 29.7$ (27.0, 32.7) s^{-1}, $\sigma = 15.2$ (12.0, 18.7) s^{-1}. The dehydrated trehalose matrices embedding the wt and the R26 RCs contained 5.2×10^3 H_2O/RC. In the RC films dehydrated in the absence of sugar, the residual water was below the detection limit of NIR spectroscopy (see Materials and Methods for further details).

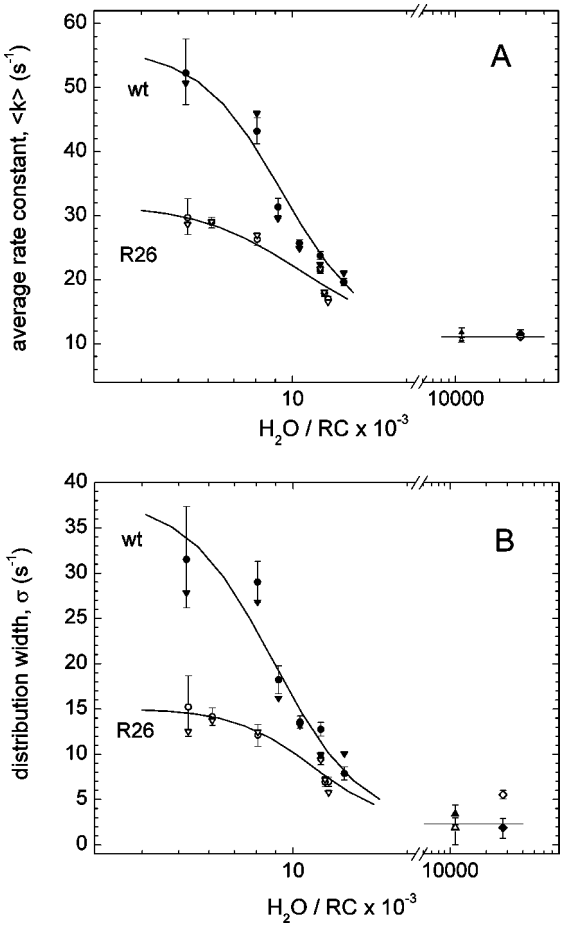

Figure 2. Dependence of the kinetics of $P^+Q_A^-$ recombination upon the content of residual water (H_2O/RC molar ratio) in trehalose−water glassy matrices incorporating the wt (filled circles) and the R26 (open circles) RCs. Measurements performed in solution in the absence of trehalose, and after redissolving the trehalose glasses are also shown with filled (wt) and open (R26) diamonds and triangles, respectively. Kinetic analysis was performed as illustrated in Figure 1 (see Materials and Methods, eqs 2−4). Values of the average rate constant $\langle k \rangle$ and of the distribution width σ are presented in panels A and B, respectively. Vertical bars indicate confidence intervals within two standard deviations (see Materials and Methods). The values at the right of the break in the abscissa scale have been obtained in solution, and the ones on the left, in glassy matrices. Values of $\langle k \rangle$ and σ evaluated by fitting the same experimental traces to a third order cumulant expansion (see Materials and Methods, eq 6) are shown for comparison with filled (wt) and open (R26) inverted triangles. Sigmoidal curves are drawn through the experimental points just to guide the eye.

(Figure 1A), reaching $\langle k \rangle$ values close to 20 s^{-1}. The rate distributions (Figure 1C) become correspondingly broader, with σ values in the range of 10 s^{-1}. In the dehydrated RC-films the kinetics of $P^+Q_A^-$ recombination appear slightly but systematically faster and more distributed in the wt than in the R26 reaction centers. This effect was reproducibly observed.

In a trehalose glassy sample, characterized by $\sim 5 \times 10^3$ residual water molecules per RC, the kinetics measured in the R26 reaction center are further accelerated, as compared to the dried RC-film, reaching a $\langle k \rangle$ value $\sim$30 s^{-1} and a σ value $\sim$15 s^{-1} (Figure 1B, D; note the different time scale in Figure 1B and 1A, as well as the different ordinate scale in Figure 1D and 1C), in agreement with previously published data.[15,18,19] In RCs from the carotenoid-containing wt, incorporated into a trehalose glass of comparable content of residual water, these effects are remarkably larger: $P^+Q_A^-$ recombination kinetics are in fact characterized by $\langle k \rangle = 52$ s^{-1} and $\sigma = 32$ s^{-1} (Figure 1D). In extensively dehydrated trehalose glasses, therefore, the $P^+Q_A^-$ state recombines almost two times faster in the wt as compared to the R26 reaction center, and the rate distribution is two times broader in the carotenoid-containing wt RC. We note that the differences found in both parameters are fully significant when considering the calculated confidence intervals within two standard deviations.

The different behaviors observed in the solid trehalose glasses led us to study systematically in the two RC types the response of $P^+Q_A^-$ recombination kinetics to a variation in the content of residual water of the embedding sugar glass. The dependences of the average rate constant $\langle k \rangle$, and of the distribution width σ, upon the H_2O/RC molar ratio are compared in Figure 2A and B, respectively, for the wt and R26 RCs incorporated into glassy matrices. The values of $\langle k \rangle$ and σ have been extracted from the kinetic traces by using two independent methods: (1) by fitting the data to a power law (eq 2), i.e. assuming that $p(k)$ is a gamma distribution (eq 3), as illustrated in Figure 1, or (2) by fitting the data to a third order cumulant expansion (eq 6). The latter approach does not require any assumption on the form of the rate distribution (except from being monomodal). As shown in Figure 2, the $\langle k \rangle$ and σ values estimated by the two methods are in excellent agreement, indicating that eq 3 is adequate to describe the rate distribution $p(k)$.

In both strains, upon decreasing the water content below about 15×10^3 water molecules per RC, the average rate constant and the distribution width undergo a steep increase. The kinetic parameters measured in the R26 and in the wt RC do not differ significantly at H_2O/RC values larger than about 10^4. However, at lower contents of the residual water, the dependences observed for the two RCs diverge progressively. A remarkably steeper increase of both $\langle k \rangle$ and σ is observed in the wt RC as compared to the R26 RC. As already noticed, at the maximal dehydration attained, corresponding to about 5000 H_2O/RC (i.e., 0.5 water per trehalose molecule), the average rate constant and the distribution width measured in the wt and R26 RC differ by a factor of 2. The effects observed in the dehydrated systems are fully reversible upon redissolving the RC−sugar matrix (see Figure 2, open triangles) and the RC film, as already reported for the R26 RC.[15,18,19]

The results described above show that in solution the $P^+Q_A^-$ state recombines essentially with the same, almost exponential kinetics in the carotenoid-containing wt and in the carotenoid-less mutant R26. This has been checked over the temperature range from −6 and +30 °C (not shown). According to the dynamic model[10] summarized in the Introduction, we argue that, in solution, both the carotenoid-containing and the carotenoid-less RC proteins undergo a fast relaxation from the *dark-adapted* to the *light-adapted* conformation and that the energy gap between the stabilized, *light-adapted* $P^+Q_A^-$ state and the ground PQ_A state is comparable in the two RC types. This is in line with the results of redox titrations of the P^+/P couple, which yielded essentially the same redox midpoint potential (E_m = 505 ± 5 mV) in the wt and R26 RCs (see Table 1), showing that the presence of the carotenoid does not affect the redox properties of the primary electron donor. The obtained E_m values are in excellent agreement with those previously determined by chemical[52] and electrochemical titrations[58] in wt RCs.

The data obtained in the dried RC films and in the trehalose matrices at different hydration levels tell us that when the RC dynamics is progressively hindered (as inferred from the accelerated and increasingly distributed kinetics of $P^+Q_A^-$ recombination), the kinetics of the wt and R26 RCs differ

TABLE 1: Midpoint Potential of the P^+/P Couple Measured under Different Conditions in Detergent Suspensions of RC from the wt 2.4.1 Strain and from the R26 Mutant

strain	additions	redox midpoint potential, E_m (mV)
wt 2.4.1	20 μM DAD, 20 μM pBQ	503 ± 5
wt 2.4.1	0.1% Triton X-100, 1 mM EDTA	503 ± 5
R26		508 ± 5
R26	20 μM DAD, 20 μM pBQ	506 ± 5

progressively. Already in the extensively dried RC films (see Figure 1A, C), the $\langle k \rangle$ and the σ values in the wt RC exceed by 16% and 25%, respectively, the corresponding parameters measured in the R26 mutant. In extensively dehydrated RC−trehalose glasses, this difference increases to 80% for $\langle k \rangle$ and 110% for the distribution width. We argue that, when severe environmental constraints affect the RC dynamics, both the relaxation to the stabilized, *light-adapted* $P^+Q_A^-$ state and the thermal fluctuations between conformational substates are hampered to a markedly different extent in the wt and R26 RCs.

Brownian Dynamics Simulations on the wt and R26 RC Protein. In order to further test and clarify the structural/dynamical origin of the different recombination kinetics observed in the mutant RC when incorporated into dry trehalose matrices, we carried out a theoretical analysis of the internal mechanics of the wt and R26 RC proteins. Brownian dynamics simulations on coarse-grained representations of bacterial RC proteins have been able to account for an increased flexibility of RC mutants, experimentally demonstrated by elastic and quasi-elastic neutron scattering data.[53] This simulative approach[55,59] can provide insight into the local mechanical properties of the protein at the level of single residues, yielding rigidity profiles, i.e. effective force constants calculated for each residue from the fluctuations of the mean distance between each amino acid residue and the remaining residues in the protein (see the Materials and Methods for the details of the simulation procedure).

The results of simulations obtained from the crystallographic structures of wt (pdb 2j8c)[37] and R26 (pdb 1rg5)[38] RCs are summarized in Figure 3. The upper lines in panels A and B are the rigidity profiles for the L and M subunits, respectively, of the wt RC; the lower lines represent the difference for any residue between the effective force constants calculated for the R26 mutant and that of the wt RC. We do not show the rigidity profile of the H subunit, because it is much more flexible than the L and M subunits (with force constants that do not exceed 50 kcal mol^{-1} $Å^{-2}$), and no significant variations were found between the wt RC and R26 mutant. The profiles of the wt L and M subunits are very similar to the ones already published for the same RC,[53] starting from a different crystallographic structure (pdb 1k6l).[60] As already noticed, regions close to the nonheme iron atom (L180-L195, L225-L240, M210-M230, and M260-M275) exhibit the largest rigidity. The lower curves in Figure 3 show that the R26 reaction center is considerably more flexible than the wt RC. More specifically, the largest decrease in the calculated force constants occurs for residues in the more rigid region of the protein (notably for residues M216, M217, M219, and M222), located on the quinone acceptor side of the RC. In the same region, other residues undergo a significant decrease in the force constant (L187, L188, L190, L240, M211, M214, M215, M218, M220, M221, M223, M224, M232, M234, M269, and M273).

The higher local rigidity of the wt RC revealed by Brownian dynamics simulations is fully consistent with the larger inhibition

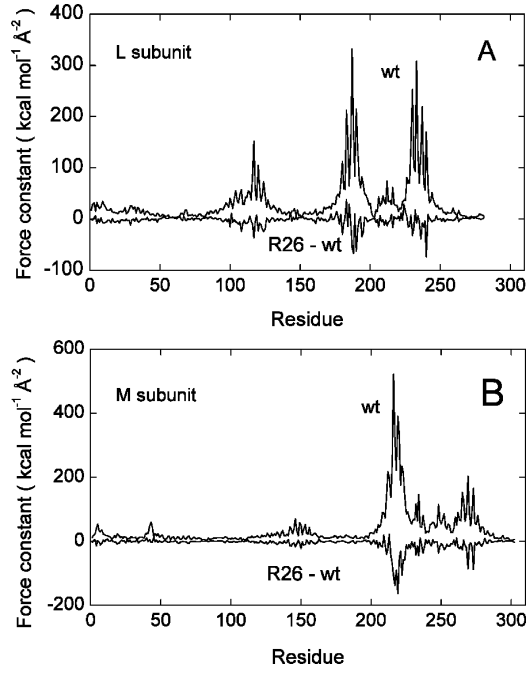

Figure 3. Comparison between the local rigidity of the wt and of the R26 reaction centers as evaluated from the results of Brownian dynamics simulations. Effective force constant profiles are shown for the residues belonging to the L (panel A) and to the M (panel B) subunits of the RC. In each panel, the upper curves refer to the profile calculated for the wt RC, while the lower curves represent the difference between the effective force constant calculated in the R26 RC and in the wt RC.

of the wt RC internal dynamics, as probed by the kinetics of $P^+Q_A^-$ recombination in dried RC−trehalose glasses (see Discussion).

Discussion

The kinetic analysis of $P^+Q_A^-$ decay shows that, in extensively dehydrated RC−trehalose glasses, characterized by a comparable content of residual water, recombination occurs two times faster in the wt RC than in the carotenoid-less R26 mutant. Moreover, in the wt RC the rate distribution is more than two-times broader. From the former observation we infer that, over the time scale of charge recombination, the flash-induced $P^+Q_A^-$ state is less stabilized in the wt than in the R26 RCs. The broader rate distribution in the wt RC also tells us that in trehalose glasses the wt RC is trapped over a larger ensemble of substates as compared to the R26 RC. Taken together, the two observations indicate that in the extensively dehydrated trehalose glasses the internal protein dynamics probed by $P^+Q_A^-$ recombination kinetics is more severely hindered in the carotenoid-containing wt RC. Specifically, this implies that, in the wt RC, trehalose-coating causes a more efficient trapping of the unrelaxed, *dark adapted* $P^+Q_A^-$ conformation and of the static structural heterogeneity of the protein. In the R26 mutant, at variance, a residual internal dynamics would be present even in the driest trehalose matrices, which would partially stabilize the $P^+Q_A^-$ recombination kinetics and lead to a partial averaging over the conformational substates that determine the rate distribution.

In principle, the extensive drying of the trehalose−RC glasses could affect differently in the two RC types not only the internal protein dynamics but also the energy gap between the *dark-adapted* $P^+Q_A^-$ and the PQ_A ground state. In the frame of the model adopted,[10] a larger energy gap in the wt as compared to the R26 RC would give rise to a faster charge recombination

in the wt RC. Inhibition of protein dynamics in room temperature dehydrated trehalose glasses implies that the energy barriers between protein conformational states and substates are dramatically increased.[15,17,18] Alterations of the internal protein dynamics and of the protein energy landscapes are therefore constitutively interconnected, making possible that a larger energy gap between the *dark-adapted* $P^+Q_A^-$ and the PQ_A ground state in the solid glass also contributes to accelerate charge recombination in the wt RC. We note, however, that the large broadening of the rate distribution function in the wt, as compared to the R26 RC, indicates, in the former RC type, a stronger inhibition of the internal protein dynamics which determines the interconversion between conformational substates. This observation strongly favors a predominantly dynamic origin of the different recombination kinetics observed in the solid trehalose glasses, since there is no *a priori* reason for assuming a different static heterogeneity in the two RC types.

In moderately dehydrated trehalose glasses and in RC-film dried in the absence of sugar, the differences observed in the recombination kinetics between the wt and R26 RCs are less pronounced. This is consistent with the notion that, when the dynamics of the RC protein is less inhibited, relaxation to the *light-adapted* state and interconversion between substates can occur over a time scale comparable with that of charge recombination both in the wt and in the R26 RCs. Under these conditions, as expected, the kinetics of charge recombination become less sensitive to differences in the internal protein dynamics between the two RC types. No significant differences in the kinetics can be detected between the two RCs in solution. Narrow rate distributions are found (almost-exponential kinetics), indicating that interconversion between conformational substates takes place rapidly enough over the time of charge recombination to average the static heterogeneity in both RCs. The very close values of $\langle k \rangle$ show moreover that the energy gap between the relaxed *light-adapted* $P^+Q_A^-$ state and PQ_A is the same in the wt and in the R26 mutant. This is in accordance with the coincident values found for the redox midpoint potential of the primary donor P^+/P couple in the two RCs.

According to the *anchorage* model of the trehalose−protein interaction, incorporation of the protein into the sugar matrix and dehydration of the system results in the formation of an hydrogen bond network, which connects surface groups of the protein, via molecules of residual water, to the trehalose matrix.[19,20,33] In strongly dehydrated glasses, this network reduces dramatically the motional freedom of the protein surface. The inhibition of *internal* motions within the protein is expected therefore to depend upon the local, *internal* rigidity of the protein. In fact, the internal mechanical properties of the protein will determine the range and extent of propagation of the mechanical constraints introduced by the sugar matrix at the protein surface. The *anchorage* model, therefore, implies that the stronger structural/dynamical protein−matrix coupling revealed in the wt RC−trehalose glasses by the kinetics of charge recombination reflects a larger internal rigidity of the wt RC protein as compared to the R26 mutant. This conclusion is fully consistent with the results of Brownian dynamics simulations carried out in the present study.

Brownian dynamics simulations performed on reduced protein representations have proven to be a useful tool to analyze protein mechanical properties on a residue-by-residue basis.[59] This approach has been recently applied to a variety of proteins, including hemoproteins[55] and the photosynthetic reaction center.[53]

The force constant profiles calculated for the wt RC from the pdb structure 2j8c[37] (Figure 3) agree well with the rigidity profiles previously obtained from a different crystallographic structure (pdb file 1k6l)[60] of the same RC protein, showing in particular a rigid core located in the vicinity of the nonheme iron atom. When the force constant profile is calculated for the R26 mutant, it appears that this protein is more flexible than the wt and that the largest variations of the force constants occur within the most rigid core of the RC. The force constant profiles shown in Figure 3 have been calculated in the absence of cofactors; that is, the carotenoid molecule was not taken into account in the structure of the wt RC. The inclusion of the prosthetic groups did not change significantly the results of the simulation, in agreement with what was found previously for the other proteins studied.[55,61] This means that the softening of the R26 RC evidenced by the simulations is an intrinsic mechanical property of the apoprotein architecture. The different "rigidity" derives uniquely from the relatively small differences, revealed by the crystallographic data, in the conformational structure of the two proteins in response to the presence/absence of the carotenoid molecule. Following structural alignment of the two RCs, the overall Cα rmsd between the wt and the R26 L and M subunit structures, calculated over the residues included in the Brownian dynamics simulations, results in a value of 0.75 Å.

It is worth mentioning that the larger compactness of the wt compared to the R26 structure appears directly in the spring networks built from the crystallographic data. The reduced model resulting from the wt crystallographic structure (2j8c)[37] is made of 1822 pseudoatoms and 29152 springs, while the one constructed from the R26 structure (1rg5)[38] comprises 1826 pseudoatoms and 27505 springs. In accordance with the lower number of springs in the R26 representation, analysis of the RC cavities based on the two RC structures reveals a significantly larger internal void volume of the R26 structure as compared to the wt. The less dense structure of the R26 mutant is in line with comparative high pressure studies which suggest a larger compressibility of the carotenoid-less mutant.[39,40] Recently, Scherz and co-workers[62] showed that single point mutations at the D1-212 residue of the cyanobacterial PSII reaction center substantially affect the rate of Q_A^- to Q_B electron transfer, specifically altering the activation entropy of the reaction. Interestingly, based on a thorough *in silico* analysis of the available PSII structures, the authors provide evidence that movements or changes in the size of this residue alter the volume and shape of protein cavities conserved in the PSII structure, modifying the local flexibility of the reaction center.[62]

The location of the residues which in the R26 protein undergo a more pronounced softening is shown by van der Waals envelopes in Figure 4. The largest changes in force constant (between −100 and −165 kcal mol^{-1} $Å^{-2}$) occur for residues (PheM216, AlaM217, HisM219, ThrM222), shown in red in Figure 4, which belong to the M subunit, to which the carotenoid molecule is bound in the wt structure. These residues form a cluster with 12 additional residues of the M subunit and with 4 residues of the L subunit (orange colored in Figure 4), for which the force constant undergoes smaller variations (between −40 and −100 kcal mol^{-1} $Å^{-2}$). We notice that three of the residues which exhibit a significant variation in the force constant (HisM219, GluM234, and HisL190) act as ligands of the iron atom.

The cluster of residues which becomes more flexible in the R26 RC is at a considerable distance from the position occupied by the carotenoid molecule in the wt structure (the minimal

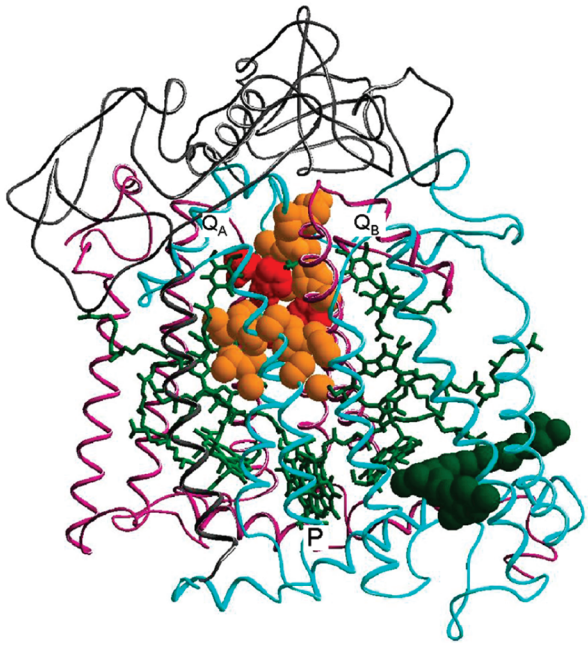

Figure 4. Localization of the residues which undergo significant changes in rigidity when passing from the wt to the R26 RC. A ribbon representation of the L (pink), M (blue), and H (gray) subunits of the wt RC (pdb structure 2j8c)[37] is shown, with the cofactors in green. van der Waals envelopes represent the carotenoid molecule (green), which is absent in the R26 RC, and the residues which undergo significant changes of the effective force constant in the R26 as compared to the wt RC. Residues characterized by the largest variations of the force constant (between −100 and −165 kcal mol^{-1} $Å^{-2}$) are shown in red. Those which exhibit a variation between −40 and −100 kcal mol^{-1} $Å^{-2}$ are colored in orange.

edge-atom to edge-atom distance between the carotenoid and the closer residue of the cluster (AlaL188) is 19 Å). The simulations evidence therefore that the subtle structural rearrangements induced by removal of the carotenoid molecule cause long-range variations in the mechanical properties of the RC protein. A similar long-range softening effect has been found by Brownian dynamics simulation when comparing the rigidity profiles calculated for the wt RC with those of a nonfunctional mutant carrying the mutations GluL212/AspL213→Ala/Ala.[53] Also in this case the mutations mainly affect a cluster of residues which belong to the most rigid region of the RC around the iron atom and which are on average relatively distant (above 15 Å) from the site of the point mutations. Comparably long-range dynamic effects of single-site mutations have been recently reported for soluble proteins (see e.g. refs 63 and 64).

When the experimental results we obtained in the trehalose−RC glasses are considered in the light of the information provided by the Brownian dynamics simulations, it appears that softening of a cluster of residues in the R26 RC protein can loosen the structural/dynamical coupling between the RC−trehalose−water matrix and the site(s) of the RC protein involved in relaxation of the $P^+Q_A^-$ state from the *dark adapted* to the *light-adapted* conformation. Interestingly, the high resolution structure of the wt RC by Fritzsch and co-workers[37] reveals that most of the residues which undergo a rigidity change in the R26 mutant are part of an hydrogen bond network which also involves a large number of bound water molecules and a few additional residues very close to the surface of the protein. It seems reasonable therefore to propose that through this hydrogen bond network the altered force constants of a limited number of key residues can affect the dynamics which govern charge recombination, by loosening or tightening the mechanical coupling between the protein surface locked by the trehalose glass and the residue(s) buried within the protein, involved in the relevant conformational change(s).

The largest differences in force constants between the wt and the R26 are found for residues which cluster around the quinone acceptor complex. This suggests that the conformational changes induced by the formation of the charge separated state $P^+Q_A^-$ are localized on the quinone acceptor side of the RC and involve the binding pocket of Q_A. FTIR studies performed on the *Rb. sphaeroides* RC have shown that formation of the $P^+Q_A^-$ state is associated with a light-induced differential band at 1650 cm^{-1}, most likely reflecting some change in a peptide C═O vibration belonging to the Q_A binding pocket.[6] The authors propose that the involved residue is possibly an alanine (Ala M260), which is conserved in *Rhodopseudomonas viridis*. The peptide nitrogen of this residue is within hydrogen bonding distance from one of the C═O groups of Q_A. As noticed by the authors, the conformational change could alternatively involve ThrM222, which is also at hydrogen bond distance from the other C═O group of Q_A in *Rb. sphaeroides*. Notably, Brownian dynamics simulations predict a large decrease (−105 kcal mol^{-1} $Å^{-2}$) for this residue in the R26 mutant as compared to the wt. In agreement with a localization of the conformational change near the Q_A binding pocket, in a recent FTIR study, isotope-shifted water bands were observed after formation of Q_A^-, indicating the presence of weakly hydrogen bonded water molecules near Q_A whose spectra are perturbed by quinone reduction.[65] The authors propose that a conformational change due to the reorientation of weakly hydrogen bonded water contributes to the stabilization of the primary charge separated state, as probed by $P^+Q_A^-$ recombination kinetics.

Conclusions

The reported results have a number of general implications which concern how local structural changes can affect protein dynamics and how structural/dynamical constraints introduced at the protein surface can alter the dynamics of residues deeply buried within the protein. The combined experimental and computational analysis presented here points to the following main conclusions:

(i) The effects of limited structural changes on protein flexibility can be unexpectedly complex and long-range; in fact, removal of the carotenoid molecule from the RC appears to induce a protein rearrangement which affects substantially the RC dynamics, mainly altering the rigidity of residues located at more than 20 Å from the carotenoid. This is in line with the results of a study in which the dynamical long-range effects of single point mutations on the RC dynamics have been examined experimentally by neutron scattering and computationally by coarse-grained Brownian simulations.[53]

(ii) The spatial constraints introduced at the protein surface by incorporation of the RC into extensively dehydrated trehalose matrices can inhibit internal motions which involve buried residues; the extent and specificity of this motional hindrance appear to be determined by the local, internal mechanical properties of the protein. This notion is consistent with the proposal (*anchorage hypothesis*) that the dynamical inhibition, and the consequent bioprotective effects, induced by the trehalose coating are due to the formation of a water-mediated hydrogen bond network which anchors the protein surface to the surrounding environment.

(iii) The structural rearrangement stabilizing the light-induced $P^+Q_A^-$ state (inhibited in the solid trehalose glass) is localized

on the quinone acceptor side of the RC, in the vicinity of the Q_A binding pocket. This is suggested by the comparison of the rigidity profiles of the wt and R26 mutant, which show that most of the residues undergoing the largest differences in the calculated force constant belong to the M subunit and cluster around the nonheme iron atom.

We think to be particularly relevant that coarse-grained Brownian dynamics simulations give a picture of the RC mechanical properties at the residue level, which is consistent with the effects experimentally observed in dehydrated trehalose matrices on a specific electron transfer process. The combination of this experimental approach with computational methods appears to be promising in examining a number of available RC mutants, for which the effects of point mutations on the protein dynamics have been scarcely considered.

Acknowledgment. This work was financially supported by MIUR of Italy and CNRS of France. We acknowledge stimulating discussions with Paola Turina, Andreas Labahn, Pierre Sebban, and Lorenzo Cordone. We also would like to thank B. Andrea Melandri and Klaus Möbius for helpful suggestions and critical reading of the manuscript.

References and Notes

(1) Feher, G.; Allen, J. P.; Okamura, M. Y.; Rees, D. C. *Nature* **1989**, *33*, 111.
(2) Hoff, A. J.; Deisenhofer, *J. Phys. Rep.* **1997**, *287*, 1.
(3) Okamura, M. Y.; Paddock, M. L.; Graige, M. S.; Feher, G. *Biochim. Biophys. Acta* **2000**, *1458*, 148.
(4) McElroy, J. D.; Mauzerall, D. C.; Feher, G. *Biochim. Biophys. Acta* **1974**, *333*, 261.
(5) Kleinfeld, D.; Okamura, M. Y.; Feher, G. *Biochemistry* **1984**, *23*, 5780.
(6) Nabedryk, E.; Bagley, K. A.; Thibodeau, D. L.; Bausher, M.; Mäntele, W.; Breton, J. *FEBS Lett.* **1990**, *266*, 59.
(7) Brzezinski, P.; Okamura, M. Y.; Feher, G. In *The Photosynthetic Bacterial Reaction Center II. Structure, Spectroscopy and Dynamics*; Breton, J., Verméglio, A., Eds.; Plenum Press: New York, 1992; pp 321−330.
(8) Brzezinski, P.; Andréasson, L.-E. *Biochemistry* **1995**, *34*, 7498.
(9) Ortega, J. M.; Mathis, P.; Williams, J. C.; Allen, J. P. *Biochemistry* **1996**, *35*, 3354.
(10) McMahon, B. H.; Müller, J. D.; Wraight, C. A.; Nienhaus, G. U. *Biophys. J.* **1998**, *74*, 2567.
(11) Edens, G. J.; Gunner, M. R.; Xu, Q.; Mauzerall, D. *J. Am. Chem. Soc.* **2000**, *122*, 1479.
(12) Xu, Q.; Gunner, M. R. *J. Phys. Chem. B* **2000**, *104*, 8035.
(13) Kriegl, J. M.; Nienhaus, G. U. *Proc. Natl. Acad. Sci. U.S.A.* **2004**, *101*, 123.
(14) Kriegl, J. M.; Forster, F. K.; Nienhaus, G. U. *Biophys. J.* **2003**, *85*, 1851.
(15) Palazzo, G.; Mallardi, A.; Hochkoeppler, A.; Cordone, L.; Venturoli, G. *Biophys. J.* **2002**, *82*, 558.
(16) Graige, M. S.; Feher, G.; Okamura, M. Y. *Proc. Natl. Acad. Sci. U.S.A.* **1998**, *95*, 11679.
(17) Francia, F.; Palazzo, G.; Mallardi, A.; Cordone, L.; Venturoli, G. *Biophys. J.* **2003**, *85*, 2760.
(18) Francia, F.; Palazzo, G.; Mallardi, A.; Cordone, L.; Venturoli, G. *Biochim. Biophys. Acta* **2004**, *1658*, 50.
(19) Francia, F.; Dezi, M.; Mallardi, A.; Palazzo, G.; Cordone, L.; Venturoli, G. *J. Am. Chem. Soc.* **2008**, *130*, 10240.
(20) Cordone, L.; Cottone, G.; Giuffrida, S.; Palazzo, G.; Venturoli, G.; Viappiani, C. *Biochim. Biophys. Acta* **2005**, *1749*, 252.
(21) Cottone, G.; Cordone, L.; Ciccotti, G. *Biophys. J.* **2001**, *80*, 931.
(22) Hagen, S. J.; Hofrichter, J.; Eaton, W. A. *Science* **1995**, *269*, 959.
(23) Hagen, S. J.; Hofrichter, J.; Eaton, W. A. *J. Phys. Chem.* **1996**, *100*, 12008.
(24) Cordone, L.; Galajda, P.; Vitrano, E.; Gassmann, A.; Ostermann, A.; Parak, F. *Eur. Biophys. J.* **1998**, *27*, 173.
(25) Cordone, L.; Ferrand, M.; Vitrano, E.; Zaccai, G. *Biophys. J.* **1999**, *76*, 1043.
(26) Giuffrida, S.; Cottone, G.; Librizzi, F.; Cordone, L. *J. Phys. Chem. B* **2003**, *107*, 13211.
(27) Giachini, L.; Francia, F.; Cordone, L.; Boscherini, F.; Venturoli, G. *Biophys. J.* **2007**, *92*, 1350.
(28) Carpenter, J. F.; Crowe, J. H. *Biochemistry* **1989**, *28*, 3916.
(29) Allison, S. D.; Chang, B.; Randolph, T. W.; Carpenter, J. F. *Arch. Biochem. Biophys.* **1999**, *365*, 289.
(30) Belton, P. S.; Gill, A. M. *Biopolymers* **1994**, *34*, 957.
(31) Sampedro, J. G.; Uribe, S. *Mol. Cell. Biochem.* **2004**, *256*, 319.
(32) Cottone, G.; Ciccotti, G.; Cordone, L. *J. Chem. Phys.* **2002**, *117*, 9862.
(33) Giuffrida, S.; Cottone, G.; Cordone, L. *Biophys. J.* **2006**, *91*, 968.
(34) Conrad, P. B.; de Pablo, J. J. *J. Phys. Chem. A* **1999**, *103*, 4049.
(35) Ekdawi-Sever, N. C.; Conrad, P. B.; de Pablo, J. J. *J. Phys. Chem. A* **2001**, *105*, 734.
(36) Massari, A. M.; Finkelstein, I. J.; McClain, B. L.; Goj, A.; Wen, X.; Bren, K. L.; Loring, R. F.; Fayer, M. D. *J. Am. Chem. Soc.* **2005**, *127*, 14279.
(37) Koepke, J.; Krammer, E. M.; Klingen, A. R.; Sebban, P.; Ullmann, G. M.; Fritzsch, G. *J. Mol. Biol.* **2007**, *371*, 396.
(38) Roszak, A. W.; McKendrick, K.; Gardiner, A. T.; Mitchell, I. A.; Isaacs, N. W.; Cogdell, R. J.; Hashimoto, H.; Frank, H. A. *Structure* **2004**, *12*, 765.
(39) Gall, A.; Ellervee, A.; Bellisent-Funel, M. C.; Robert, B.; Freiberg, A. *Biophys. J.* **2001**, *80*, 1487.
(40) Gall, A.; Ellervee, A.; Robert, B.; Freiberg, A. *FEBS Lett.* **2004**, *560*, 221.
(41) Baciou, L.; Michel, H. *Biochemistry* **1995**, *34*, 7967.
(42) Gray, K. A.; Farchaus, J. W.; Wachtveitl, J.; Breton, J.; Oesterhelt, D. *EMBO J.* **1990**, *9*, 2061.
(43) Wraight, C. A. *Isr. J. Chem.* **1981**, *21*, 348.
(44) Sloten, L. *Biochim. Biophys. Acta* **1972**, *275*, 208.
(45) Steinbach, P. J.; Chu, K.; Frauenfelder, H.; Johnson, J. B.; Lamb, D. C.; Nienhaus, G. U.; Sauke, T. B.; Young, R. D. *Biophys. J.* **1992**, *61*, 235.
(46) Abramowitz, M.; Stegun, I. A. *Handbook of Mathematical Functions*; Dover Publications: New York, 1965.
(47) Bevington, P. R. *Data Reduction and Error Analysis for the Physical Sciences*; McGraw-Hill: New York, 1969.
(48) Beechem, J. M. *Methods Enzymol.* **1992**, *20*, 37.
(49) Holzwarth, A. R. In *Biophysical Techniques in Photosynthesis*; Amesz, J., Hoff, A. J., Eds.; Kluwer Academic Publishers: Dordrecht, The Netherland, 1996; pp 75−92.
(50) Hochkoeppler, A.; Zannoni, D.; Venturoli, G. *Biochim. Biophys. Acta* **1995**, *1229*, 81.
(51) O'Reilly, J. E. *Biochim. Biophys. Acta* **1973**, *292*, 509.
(52) Williams, J. C.; Alden, R. G.; Murchison, H. A.; Peloquin, J. M.; Woodbury, N. W.; Allen, J. P. *Biochemistry* **1992**, *31*, 11029.
(53) Sacquin-Mora, S.; Sebban, P.; Derrien, V.; Frick, B.; Lavery, R.; Alba-Simionesco, C. *Biochemistry* **2007**, *46*, 14960.
(54) Zacharias, M. *Protein Sci.* **2003**, *12*, 1271.
(55) Sacquin-Mora, S.; Lavery, R. *Biophys. J.* **2006**, *90*, 2706.
(56) Tozzini, V. *Curr. Opin. Struct. Biol.* **2005**, *15*, 144.
(57) Ermak, D. L.; McCammon, J. A. *J. Chem. Phys.* **1978**, *69*, 1352.
(58) Lin, X.; Murchison, H. A.; Nagarajan, V.; Parson, W. W.; Allen, J. P.; Williams, J. C. *Proc. Natl. Acad. Sci. U.S.A.* **1994**, *91*, 10265.
(59) Lavery, R.; Sacquin-Mora, S. *J. Biosci.* **2007**, *32*, 891.
(60) Pokkuluri, P. R.; Laible, P. D.; Deng, Y. L.; Wong, T. N.; Hanson, D. K.; Schiffer, M. *Biochemistry* **2002**, *41*, 5998.
(61) Sacquin-Mora, S.; Laforet, E.; Lavery, R. *Proteins* **2007**, *67*, 350.
(62) Shlyk-Kerner, O.; Samish, I.; Kaftan, D.; Holland, N.; Maruthi Sai, P. S.; Kless, H.; Scherz, A. *Nature* **2006**, *442*, 827.
(63) Falconi, M.; Stroppolo, M. E.; Cioni, P.; Strambini, G.; Sergi, A.; Ferrario, M.; Desideri, A. *Biophys. J.* **2001**, *80*, 2556.
(64) Ceruso, M. A.; Grottesi, A.; Di Nola, A. *Proteins* **2003**, *50*, 222.
(65) Iwata, T.; Paddock, M. L.; Okamura, M. Y.; Kandori, I. *Biochemistry* **2009**, *48*, 1220.

JP902287Y